Experimental and first-principles determination of the magnetocrystalline anisotropy in Mn_xGa

Xubo Liu,[1] D. H. Ryan,[1] Manli Wang,[2] Qingmei Lu,[2] Hongguo Zhang,[2] Ming Yue,[2] and Z. Altounian[1]
[1]*Physics Department and Centre for the Physics of Materials, McGill University, 3600 University Street, Montreal, Quebec H3A 2T8, Canada*
[2]*College of Materials Science and Engineering, Beijing University of Technology, Beijing 100122, China*

(Presented 1 November 2016; received 5 September 2016; accepted 30 October 2016; published online 20 January 2017)

Singular point detection (SPD) for the determination of the anisotropy field (B_A) using a conventional magnetometer is demonstrated. We then follow the composition dependence of B_A in Mn_xGa using a combination of SPD measurements complemented by first-principles density functional theory (DFT) calculations. We find excellent quantitative agreement for $1.2 \leq x \leq 1.8$, but observe a marked departure for $x \leq 1.2$. We suggest that the deviation from ideal behaviour might be associated with site disorder at low excess Mn. [http://dx.doi.org/10.1063/1.4974890]

I. INTRODUCTION

Manganese-based magnetic compounds are being investigated for two main reasons: (1) they avoid the need for rare earths, (2) they offer a modest-cost/modest performance alternative to the two dominant hard magnet technologies based on $Nd_2Fe_{14}B$ (515 kJ m^{-3}) and $Ba(Sr)Fe_{12}O_{19}$. One possible such system is Mn-Ga. Unfortunately, the Mn-Ga binary phase diagram is extremely complex, lacking a single congruently-melting compound. As a result, sample preparation is complex and quality is often poor. In order to assess the possible applications of Mn_xGa as a new, rare-earth free hard magnetic material it is essential to start by establishing the intrinsic properties of well characterised single-phased materials as these parameters ultimately set the limits on what might be achieved through appropriate optimisation through doping and heat treatments.

In our previous work on the Mn_xGa hard magnet system we concentrated on the crystal structure and basic magnetic properties (T_c and saturation magnetisation).[1–3] We showed that the system adopts a primitive tetragonal structure (P4/*mmm* #123, sometimes denoted "$L1_0$") with Mn on the 1*d* site and a mixture of Ga and Mn on the 1*a* site, and ruled out the larger body-centred tetragonal structure (I4/*mmm* #139 sometimes denoted "$D0_{22}$").[2] Antiparallel coupling between the substitutional Mn(1*a*) moments and those on the Mn(1*d*) atoms leads to a reduction in magnetisation with increasing *x*.

Here we turn our attention to another intrinsic property of the Mn_xGa system: The anisotropy field (B_A). While the coercivity (B_c) is a key limiter for applications, it is an extrinsic materials property affected by the sample's preparation history and microstructure. By contrast, B_A is intrinsic and ultimately sets a hard upper limit on any possible coercivity. For example, in an isotropic system of non-interacting particles, the Stoner-Wohlfarth model gives $B_c \sim \frac{1}{2}B_A$.[4] Real materials often fall far short of this limit. Our work here provides a baseline for doping-based enhancements. We use two complementary techniques: (1) direct measurement by singular point detection (SPD);[5] (2) First-principles density functional theory (DFT) calculations, the results of which have been shown to yield excellent agreement with Mn moments measured by neutron diffraction.[2]

II. EXPERIMENTAL METHODS

The series of tetragonal Mn_xGa (x=1.15, 1.20, 1.40, 1.50, 1.60 and 1.80) alloys studied here are the same ones used previously in our neutron diffraction work[2] and have therefore been fully characterised. We will not repeat the various structural and magnetic properties here.[1–3] The samples were prepared by induction melting high purity gallium (99.9%) and manganese (99.5%) in an argon atmosphere. Excess Mn was added to compensate for evaporation losses during melting, and the as-cast ingots were annealed at temperatures between 700 K to 900 K for one to seven days and then quenched into ice water.

A. Singular point detection

Measurement of the anisotropy field (B_A) via singular-point detection[5,6] is conventionally carried out using pulsed high magnetic fields,[7] in large part because B_A tends to be quite large in systems of interest, but also because the SPD technique requires access to the second or third derivatives of the magnetisation with respect to the applied field[5–7] and these are relatively easy to obtain in the rapidly changing fields produced in a pulsed magnet. While Turilli showed in 1994 that the combination of a small modulating field and lock-in detection of the harmonic response could be used to measure B_A in a more conventional magnet,[8] this idea does not appear to have been picked up.

The advent of commercial, automated magnetometer/susceptometer units based around large-field superconducting magnets (such as the Quantum Design Physical Properties Measurement System "PPMS" used here) opened up the possibility of using SPD techniques in almost any laboratory. Direct, double differentiation of the magnetisation to obtain $d^2\sigma/dB^2$ places inordinate precision requirements on the magnetometer, especially since the derivatives become quite small as the system approaches saturation (where B_A is inevitably located). Increasing the sample size to compensate, just overloads the detection system. However, if one simply measures the ac susceptibility, $\chi_{ac} = d\sigma/dB$, and then differentiates numerically to obtain $d^2\sigma/dB^2$, the resulting signal is remarkably clean.

Figure 1 shows some typical data for $Mn_{1.2}Ga$ taken at 200 K. The sample size used (about 40 mg) was close to saturating the magnetometer, but the susceptibility is far below the saturation limits of the instrument and much larger samples could be used if signal strength is problematic. The magnetisation curve in Figure 1 shows the usual slow approach to saturation typical of these

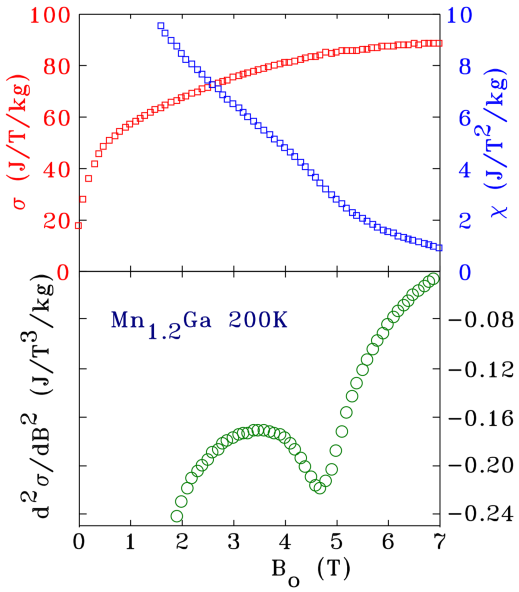

FIG. 1. Top: Magnetisation (red points, left axis) and susceptibility (blue points, right axis) for $Mn_{1.2}Ga$ at 200 K, obtained by direct measurement using a Quantum Design PPMS. The approach to saturation is quite slow and there is a weak inflection in the $\chi(B_o)$ trend. This inflection is more clearly seen in the numerically calculated second derivative of the magnetisation shown in the lower panel. The minimum in $d^2\sigma/dB^2$ at $B_o = 4.70(7)$T marks the anisotropy field (B_A).

materials. The ac susceptibility measured at 1 kHz with a drive field of 1 mT shows a steady decline (the low-field section has been removed to permit re-scaling) but an inflection is apparent near B_o=5 T. Numerical differentiation yields $d^2\sigma/dB^2$ which exhibits a very well defined cusp at B_A=4.70(7) T. We used a 3-point low-noise Lanczos differentiator with $M = 2$ (a quadratic fit),[9] but the susceptibility data were clean enough that this was almost certainly over-kill. The SPD method used here requires no special set-ups or modification of the existing system and the complete measurement can be carried out in a matter of minutes.

B. Density functional calculations

The magnetocrystalline anisotropy (MCA) is the result of an interaction between the spin-orbit coupling (SOC) and the crystal field (CF).[10] The details of MCA depend on many factors such as lattice strain or chemical composition variation.

There are several DFT-based methods for calculating the magnetocrystalline anisotropy. One is a self-consistent scheme based on the direct calculation of the total energy difference between the two different magnetisation directions with spin-orbit coupling. In principle, this approach is exact and straightforward, but it is computationally demanding. With the force theorem (FT) approach, the computational cost is substantially reduced. The MCA is taken as the band energy difference obtained after a one-step diagonalisation of the full Hamiltonian including SOC, starting from the well converged self-consistent scalar relativistic (without SOC) density/potential. In 3*d* systems, the SOC band shifts are usually well described by second-order perturbation theory. The anisotropy of the expectation value of the SOC operator $\Delta E_{soc} = \langle V_{soc}\rangle_a - \langle V_{soc}\rangle_c$ is approximately equal to $2E_{MCA}$.[11–14]

First-principles DFT calculations have been performed using the linear-muffin-tin orbitals (LMTO) method with a coherent potential approximation (CPA) to treat alloying behaviour.[15,16] The exchange-correlation has been treated by the generalised gradient approximation (GGA) of Perdew-Burke-Ernzerhof.[17] The k-space integrations have been performed with the tetrahedron method.[18,19] A uniform mesh of 24 × 24 × 24 in the full Brillouin zone provided sufficient accuracy for the k integration. The relativistic effects are treated by solving a scalar relativistic wave equation. For 3*d* system, SOC energy is relatively weak and can be treated perturbatively,[11,14] and spin-resolved electron filling near the Fermi level plays a major role in determining E_{soc}.[11,12] The MCA energy is approximately one half of the difference between the spin-orbital energy E_{SOC} with spin quantisation axis parallel to the [100] and [001] crystal orientations, i.e. $E_{MCA} = (E_{soc}^{100} - E_{soc}^{001})/2$. A positive E_{MCA} implies uniaxial magnetic anisotropy while a negative E_{MCA} indicates easy-plane magnetic anisotropy.

In our calculations, the lattice constants were derived from a linear fit to the experimental data on Mn_xGa[3]. The derived relationship between lattice constants and composition x in Mn_xGa were $a = 2.7203 + 0.02027 \cdot x$ and $c = 3.7235 - 0.13668 \cdot x$ for the P4/*mmm* structure.

III. RESULTS AND DISCUSSION

The MCA energy (E_{MCA}) has been calculated as a function of x in Mn_xGa. Figure 2(a) shows that as the excess Mn enters 1*a* site, there is an initial sharp increase in E_{MCA} followed by a more gradual increase after $x = 1.2$. To understand the origin of MCA in Mn_xGa, the atomic- and site-resolved E_{MCA} are displayed in Figure 2(b). The contribution from Mn at the 1*d* site dominates E_{MCA} and increases initially and then remains almost unchanged with increasing x. The contribution from Mn at the 1*a* site is small but negative, i.e. it tends to favour easy plane anisotropy. However, its contribution falls with increasing x, and this tends to offset the effects of an increasing population of Mn(1*a*) atoms. The contribution from Ga at the 1*a* site is small and positive but remains almost unchanged with increasing x.

To gain more insight into the origins of the MCA in Mn_xGa, E_{soc} was resolved into spin components, i.e. spin-up ($E_{soc}^{\uparrow\uparrow}$), spin-flipping ($E_{soc}^{\uparrow\downarrow}$)and spin-down ($E_{soc}^{\downarrow\downarrow}$) contributions. For Mn at the 1*d* site, all three components favour axial anisotropy, however the spin-flipping contribution ($2E_{soc}^{\uparrow\downarrow}$) dominates. Thus, spin flipping near Fermi level plays important role in the underlying mechanism of MCA in Mn_xGa. In addition, $E_{soc}^{\downarrow\downarrow}$ increases with increasing x, which is responsible for the enhancement of E_{MCA} with increasing x.

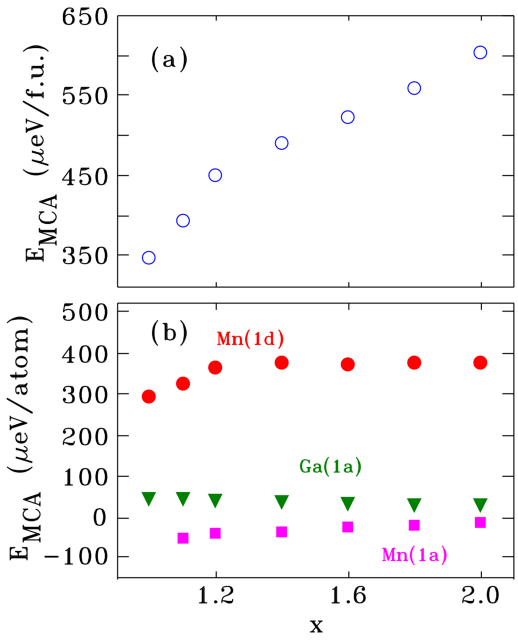

FIG. 2. (a) Calculated magnetocrystalline anisotropy energy (E_{MCA}) for MnxGa. (b) Site and atom resolved contributions to the total E_{MCA}. Note: For x=1.0 there is no Mn on the 1a site and hence no contribution.

For uniaxial anisotropy, $K_{eff} = E_{MCA}$, so the effective MCA field (B_A) has been calculated using $B_A = 2K_{eff}/\mu_0 M_s = 2E_{MCA}/\mu_0 M_s$, where M_s is the calculated saturation magnetisation. As shown in Figure 3, following an initial sharp rise, B_A increases linearly with x for $x \geq 1.1$. The agreement with the experimental results for $1.2 \leq x \leq 1.8$ is remarkably good. However there is a marked departure for $x \leq 1.2$ as the measured B_A falls well below that predicted by our DFT calculations. It is also clear from the two points measured for different (nominal) $x = 1.2$ samples that there is a significant sensitivity to composition and/or sample history in samples with a smaller excess of Mn. Given the quality of the quantitative agreement for $x > 1.2$, we are inclined to suggest that the departure for $x \leq 1.2$ represents a real effect.

One possibility lies in the idealised model used for the calculations: The excess Mn is assumed to substitute randomly for Ga on the 1a with no other effects. However, it is possible that there may

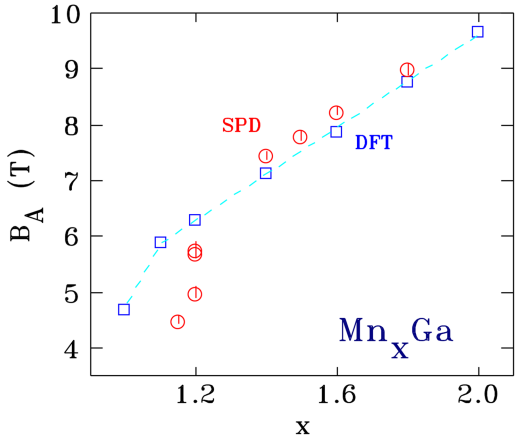

FIG. 3. Comparison of the anisotropy field for MnxGa derived from DFT calculations (blue squares) and SPD measurements at 5 K (red circles). For $x \leq 1.2$ the measured values decline more rapidly than those calculated by DFT. Data for two different $x = 1.2$ samples are shown. The dashed line follows the DFT values and is a guide to the eye.

be a tendency for the Mn to cluster, or for some Ga to be displaced onto the Mn(1*d*) sites. Given the low concentrations involved, both departures from ideality would be extremely difficult to pick up by neutron diffraction, but initial calculations suggest that this disorder effect could be the origin of the reduced magnetisation predicted by extrapolation for stoichiometric $MnGa^3$, and it might go some way to explaining the instability of the 1:1 parent compound, which so far has eluded preparation.

IV. CONCLUSIONS

We demonstrate that a conventional extraction magnetometer (Quantum Design Physical Properties Measurement System – PPMS) can be used to determine the anisotropy field (B_A) using the singular point detection method. The required second derivative of the magnetisation ($d^2\sigma/dB^2$) was obtained by numerical differentiation of the ac susceptibility ($\chi_{ac} = d\sigma/dB$) measured step-wise as a function of the applied field.

This approach is applied to the investigation of the composition dependence of B_A in Mn_xGa, a rare-earth free hard magnet system. First-principles DFT calculations indicate that the contribution from the Mn(1*d*) site dominates the MCA energy and increases with x in Mn_xGa. Despite a small negative contribution from Mn at the Ga(1*a*) site, the effective magnetic anisotropy field (B_A) increases from 4 T to 10 T as x increases from 1 to 2. The calculations are in excellent agreement with experimental values of B_A, however there is a marked departure for $x \leq 1.2$ which may be associated with site disorder at low Mn excesses.

ACKNOWLEDGMENTS

Financial support for this work was provided by: the Natural Sciences and Engineering Research Council of Canada, the Fonds Québécois de la Recherche sur la Nature et les Technologies, the State Key Program of National Natural Science Foundation of China (51331003), Beijing Natural Science Foundation (2152006), State Key Lab of Advanced Metals and Materials (2014-ZD07), the Scientific Research Foundation for the Returned Overseas Chinese Scholars, State Education Ministry, and the Fundamental Research Foundation of Beijing University of Technology. We would like to thank Quantum Design, Inc. and Randy Dumas for additional high field AC susceptibility measurements.

[1] R. Rejali, D. H. Ryan, Z. Altounian, C. Boyer, Q. Lu, M. Wang, H. Zhang, and M. Yue, AIP Advances **6**, 056003 (2016).
[2] D. H. Ryan, M. Yue, C. Boyer, X. Liu, Q. Lu, M. Wang, C. Li, H. Zhang, and Z. Altounian, Scientific Reports (submitted).
[3] Q. M. Lu, M. Yue, H. G. Zhang, M. L. Wang, F. Yu, Q. Z. Huang, D. H. Ryan, and Z. Altounian, Scientific Reports **5**, 17086 (2015).
[4] E. C. Stoner and E. P. Wohlfarth, Philosophical Transactions of the Royal Society A **240**, 599 (1948).
[5] G. Asti and S. Rinaldi, Phys. Rev. Lett. **28**, 1584 (1972).
[6] G. Asti and S. Rinaldi, J. Appl. Phys. **45**, 3600 (1974).
[7] F. Bolzoni and R. Cabassi, Physica B **346-347**, 524 (2004).
[8] G. Turilli and J. Magn, Magn. Mater. **130**, 377 (1994).
[9] P. Holoborodko, "Smooth noise robust differentiators," http://www.holoborodko.com/pavel/numerical-methods/numerical-derivative/smooth-low-noise-differentiators/ (2008).
[10] K. Yosida, K. Okiji, and S. Chikazumi, Prog. Theor. Phys. **33**, 559 (1965).
[11] K. D. Belashchenko, L. Ke, M. Däne, L. X. Benedict, T. N. Lamichhane, V. Taufour, A. Jesche, S. L. Bud'ko, P. C. Canfield, and V. P. Antropov, Appl. Phys. Lett. **106**, 062408 (2015).
[12] V. Antropov, L. Ke, and D. Aberg, Solid State Commun. **194**, 35 (2014).
[13] E. K. Delczeg-Czirjak, A. Edström, M. Werwiński, J. Rusz, N. V. Skorodumova, L. Vitos, and O. Eriksson, Phys. Rev. B **89**, 144403 (2014).
[14] L. Ke and M. van Schilfgaarde, Phys. Rev. B **92**, 014423 (2015).
[15] O. K. Andersen, Phys. Rev. B **12**, 3060 (1975).
[16] I. Turek, V. Drchal, J. Kurdnovský, M. Šob, and P. Weinberger, *Electronic Structure of Disordered Alloys, Surfaces and Interfaces* (Kluwer, Boston, 1996).
[17] J. P. Perdew, K. Burke, and M. Ernzerhof, Phys. Rev. Lett. **77**, 3865 (1996).
[18] O. Jepson and O. Anderson, Solid State Communications **9**, 1763 (1971).
[19] P. E. Blöchl, O. Jepsen, and O. K. Andersen, Phys. Rev. B **49**, 16223 (1994).